

Retinal protection by fungal product theissenolactone B in a sodium iodate-induced AMD model through targeting retinal pigment epithelial matrix metalloproteinase-9 and microglia activity

Fan-Li Lin^{a,b}, Yu-Wen Cheng^{c,1}, Li-Huei Chen^{a,b}, Jau-Der Ho^d, Jing-Lun Yen^{a,b}, Mong-Heng Wang^e, Tzong-Huei Lee^{f,1}, George Hsiao^{a,b,g,*}

^a Graduate Institute of Medical Sciences, College of Medicine, Taipei Medical University, Taipei, Taiwan

^b Department of Pharmacology, School of Medicine, College of Medicine, Taipei Medical University, Taipei, Taiwan

^c School of Pharmacy, College of Pharmacy, Taipei Medical University, Taipei, Taiwan

^d Department of Ophthalmology, Taipei Medical University Hospital, Taipei, Taiwan

^e Department of Physiology, Augusta University, Augusta, GA, USA

^f Institute of Fisheries Science, National Taiwan University, Taipei, Taiwan

^g Ph.D. Program for the Clinical Drug Discovery from Botanical Herbs, College of Pharmacy, Taipei Medical University, Taipei, Taiwan

ARTICLE INFO

Keywords:

Age-related macular degeneration
Theissenolactone B
Retina pigment epithelium
Matrix metalloproteinase-9
Microglia
NF-κB

ABSTRACT

Age-related macular degeneration (AMD) is the leading cause of low vision and blindness for which there is currently no cure. Increased matrix metalloproteinase-9 (MMP-9) was found in AMD and potentially contributes to its pathogenesis. Resident microglia also promote the processes of chronic neuroinflammation, accelerating the progression of AMD. The present study investigates the effects and mechanisms of the natural compound theissenolactone B (LB53), isolated from *Theissenia cinerea*, on the effects of RPE dysregulation and microglia hyperactivation and its retinal protective ability in a sodium iodate (NaIO₃)-induced retinal degeneration model of AMD. The fungal component LB53 significantly reduces MMP-9 gelatinolysis in TNF-α-stimulated human RPE cells (ARPE-19). Similarly, LB53 abolishes MMP-9 protein and mRNA expression in ARPE-19 cells. Moreover, LB53 efficiently suppresses nitric oxide (NO) production, iNOS expression, and intracellular ROS levels in LPS-stimulated TLR 4-activated microglial BV-2 cells. According to signaling studies, LB53 specifically targets canonical NF-κB signaling in both ARPE-19 and BV-2 microglia. In an RPE-BV-2 interaction assay, LB53 ameliorates LPS-activated BV-2 conditioned medium-induced MMP-9 activation and expression in the RPE. In NaIO₃-induced AMD mouse model, LB53 restores photoreceptor and bipolar cell dysfunction as assessed by electroretinography (ERG). Additionally, LB53 prevents retinal thinning, primarily the photoreceptor, and reduces retinal blood flow from NaIO₃ damage evaluated by optic coherence tomography (OCT) and laser speckle flowgraphy (LSFG), respectively. Our results demonstrate that LB53 exerts neuroprotection in a mouse model of AMD, which can be attributed to its anti-retinal inflammatory effects by impeding RPE-mediated MMP-9 activation and anti-microglia.

Abbreviations: AMD, age-related macular degeneration; COX-2, cyclooxygenase-2; CNV, choroidal neovascularization; ECM, extracellular matrix; ERG, electroretinography; IL, interleukin; IKK, IκB kinase; iNOS, inducible nitric oxide synthase; LB53, theissenolactone B; LPS, lipopolysaccharide; LSFG, laser speckle flowgraphy; MAPK, mitogen-activated protein kinase; MCP-1, monocyte chemoattractant protein-1; MMP, matrix metalloproteinase; NF-κB, nuclear transcription-factor kappa B; NFL, nerve fiber layer; NO, nitric oxide; OCT, optic coherence tomography; ONL, outer nuclear layer; OPL, outer plexiform layer; RPE, retinal pigmented epithelium; ROS, reactive oxygen species; TLR-4, toll-like receptor-4; TNF-α, tumor necrosis factor-α; VEGF, vascular endothelial growth factor.

* Correspondence to: Department of Pharmacology, School of Medicine, College of Medicine, Taipei Medical University, No. 250, Wu-Hsing Street, Taipei 110, Taiwan.

E-mail address: geohsiao@tmu.edu.tw (G. Hsiao).

¹ These authors contributed equally.

<https://doi.org/10.1016/j.bioph.2022.114138>

Received 30 October 2022; Received in revised form 7 December 2022; Accepted 13 December 2022

Available online 17 December 2022

0753-3322/© 2022 The Author(s). Published by Elsevier Masson SAS. This is an open access article under the CC BY license (<http://creativecommons.org/licenses/by/4.0/>).

1. Introduction

Age-related macular degeneration (AMD) is the leading cause of irreversible blindness in the global elderly population and preferentially affects the macular region of the retina. More than 170 million people worldwide are affected by AMD, and the prevalence of AMD is projected to double by 2050 as the population ages [1]. AMD can be classified as dry or wet forms. Dry AMD is characterized by deposits of drusen beneath the subretinal space between the retinal pigmented epithelium (RPE) and Bruch's membrane, contributed by dysregulated cellular control of oxidative stress, proteostasis, lipid homeostasis, and mitochondrial function, which cause subsequent RPE atrophy and photoreceptor damage [2,3]. Thereafter, dry AMD can progress to wet AMD characterized by choroidal neovascularization (CNV), with the progression of hemorrhage, lipid exudates, and fluid accumulation in the retina, ultimately resulting in retinal detachment and RPE death [4]. The advent of anti-vascular endothelial growth factor (VEGF) therapies has facilitated the management of advanced wet AMD by improving visual outcome, but there are limitations [5]. Moreover, there are no effective drugs approved for dry AMD, which accounts for at least 80 % of all AMD cases [6,7].

Matrix metalloproteinases (MMPs) are a family of zinc-containing endopeptidases that mainly digest extracellular matrix (ECM) proteins and have been reported to be involved in pathological tissue remodeling during disease states and inflammation [8]. A clinical study in subjects with AMD elucidated that MMP-9 was distinctly expressed adjacent to Bruch's membrane and RPE, blood vessels (endothelial cells) and stroma [9,10]. Significantly increased MMP-9 expression and its activity have been detected in the aqueous humor and plasma of AMD patients [8,11,12]. Vitreous MMP-9 levels have also been used as a biomarker of subretinal fluid accumulation in wet AMD [13]. Upregulation of MMP-9 at the transcriptional level is associated with increased vascular permeability and CNV in AMD development [14,15]. RPE cells are an important source of MMP-9 in the outer retinal environment, which has been implicated in Bruch's membrane defects and RPE barrier function [9,16–18], and the mobilization of angiogenic factors, including VEGF and platelet-derived growth factor, shifts the balance to a proangiogenic state [19]. MMP-9 also promotes the inflammatory condition at the locus of AMD by modulating physical barriers, enhancing inflammatory cytokine and chemokine release, and promoting chemoattractant of immune cells, especially resident retinal microglia, into the outer retina [20,21].

Recruited microglia play an important role in the neuroinflammatory etiology of AMD. In human AMD retinas, activated microglia and other immune mediators, such as immunoglobulins, complement proteins, and cytokines, have been found in or contact with drusenoid deposits and the RPE [22,23]. The microglia that accompany the choroid are the major source for proinflammatory cytokines such as interleukin (IL)-1, IL-6, and tumor necrosis factor (TNF) production in early AMD [23]. By virtue of a positive feedback mechanism, infiltrating microglia can alter RPE function, which in turn leads to disruption of immune privilege and increased chronic inflammation associated with AMD pathogenesis by further recruiting and activating immune cells and enabling new blood vessels to grow toward the retina [24].

Xylariaceae, a plant-derived bioactive fungus, has been used as a Chinese herbal medicine for the treatment of gastritis infection, cancer, and anti-aging due to its rich pharmacologic polysaccharides and alkaloids [25]. Theissenolactone C is a polyketide isolated from extracts of submerged culture of *Theissenia cinerea* 89091602, which is categorized in the genus *Xylaria* [26]. In an endotoxin-induced uveitis model, Theissenolactone C significantly reduced ocular inflammation and neuroinflammatory responses of GFAP and Iba-1 in the retina, with strong anti-microglial activities [27]. Theissenolactone C was also found to be a potent anti-MMP-9 agent that preserves retinal defects in a high IOP-induced ischemia/reperfusion injury model of glaucoma and attenuates monocytic activation *in vitro* [28]. Theissenolactone B (LB53) is

a diastereoisomer of theissenolactone C, as determined by ¹H- and ¹³C-NMR and HR-ESI-MS (MW=210) [26]. In contrast to theissenolactone C, a much higher yield of LB53 could be obtained from submerged culture of *Theissenia cinerea*. The success of theissenolactone in treating ocular diseases, including uveitis and glaucoma, via its anti-MMP-9 and anti-microglial/monocytic activities lead to the launch of this study. We investigate the therapeutic effects of LB53 in sodium iodate (NaIO₃)-induced retinal degeneration mimicking dry AMD, as well as its anti-MMP-9 activities and anti-inflammatory mechanisms in RPE and microglial cells, respectively.

2. Materials and methods

2.1. Reagents and antibodies

LB53 was provided by Professor Tzong-Huei Lee (National Taiwan University, Taiwan). The structure was determined by ¹H- and ¹³C-NMR and HR-ESI-MS (Fig. 1A), and the purity was at least 95 %. Sodium iodate (NaIO₃) (≥99.5 %; 71702), lipopolysaccharide (LPS) from *Escherichia coli* O127:B8 (L3880), and thiazolyl blue tetrazolium bromide (MTT) (M5655) were purchased from Sigma—Aldrich (St. Louis, MO). Recombinant human TNF-α (300–01 A) was purchased from PeproTech (Cranbury, NJ). Gelatin (17009–01) was purchased from Kanto Chemical. 2' 7'-dichlorodihydrofluorescein diacetate (DCFH-DA) (85155) and nitrate/nitrite colorimetric assay kits (780001) were from Cayman (Ann Arbor, MI). TRISure™ reagent was purchased from Bioline (London, UK). Agarose was purchased from GeneDirex (Las Vegas City, Nevada). GelRed™ nucleic acid gel stain was purchased from Biotium (Fremont, CA). The 2 × One-tube RT–PCR mix was from Bioman (New Taipei City, Taiwan). IKKβ (gtx105690), p38 (gtx110720), goat anti-mouse IgG (HRP) (gtx213111–01), and goat anti-rabbit IgG (HRP) (gtx213110–01) antibodies were purchased from GeneTex (Irvine, CA). MMP-9 antibody (AB19016) was purchased from Millipore (Temecula, CA). Antibodies against p-IKKα/β (2697), p-p38 (9211), p-p65 (3033), and IκBα (4812) were purchased from Cell Signaling Technology (Beverly, MA). Antibodies against p65 (NB100–56712) and COX-2 (NB100–689) antibodies were purchased from Novus Biologicals (Littleton, CO). An iNOS antibody (sc7271) was purchased from Santa Cruz (Dallas, Texas). α-Tubulin antibody (MS-581-P1) was purchased from Thermo Fisher Scientific (Waltham, MA).

2.2. Cell culture

The human RPE (ARPE-19) cell line was purchased from American Type Culture Collection (Manassas, VA) and cultured in DMEM/F12 medium; mouse BV-2 microglial cell line was a gift from Professor Wang-Wang Lin (National Taiwan University, Taiwan) and was cultured in DMEM. For general culture, cells were maintained in suitable medium containing NaHCO₃ (23.57 mM), HEPES (18 mM), penicillin (90 units/ml), streptomycin (90 μg/ml), L-glutamine (3.65 mM) and 10 % heat-inactivated fetal bovine serum (FBS) in a humidified atmosphere (95 % O₂ and 5 % CO₂) at 37 °C. Cells were seeded in medium containing 0.5 % FBS overnight before further assays. The culture conditions and treatments have been previously described [29].

2.3. Gelatin zymography analysis

MMP-9 activities in conditioned medium were evaluated by gelatin zymography as previously described [30]. The white bands in the brilliant blue G solution-stained gel represent MMP-9 gelatinolysis activity. An IP-008-SP Photoprint digital imaging system (Marne La Vallee, France) was used to capture images.

2.4. MTT assay

Cell viability was measured using a colorimetric MTT assay. In brief,

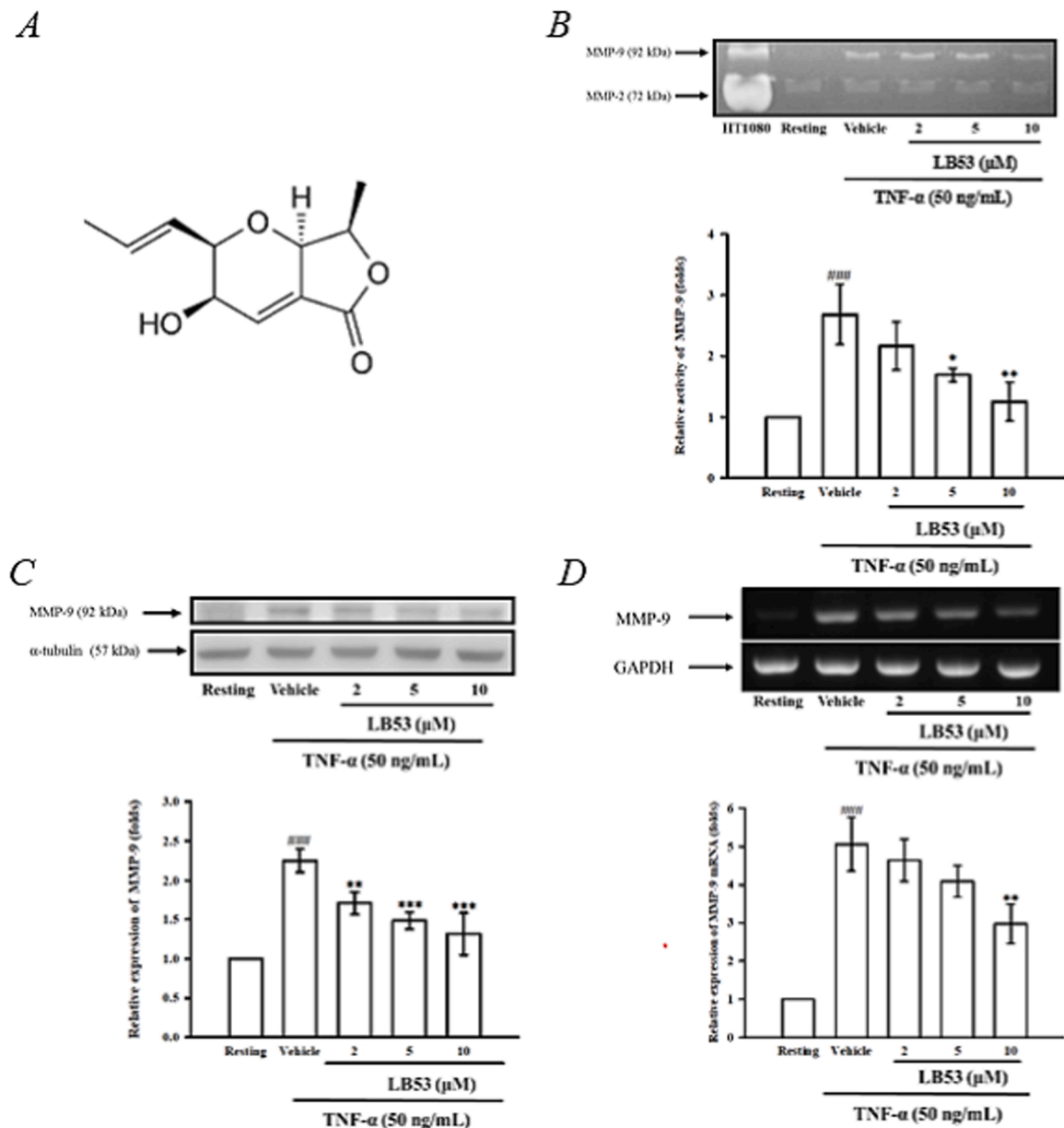


Fig. 1. Effects of LB53 on TNF- α -induced MMP-9 activation and expression in ARPE-19 cells. (A) The chemical structure of LB53 (MW = 210). (B, C) ARPE-19 cells (3×10^5 cells/ml) were seeded in 12-well plates. After pretreatment with LB53 (2, 5 and 10 μ M) or vehicle for 30 min, ARPE-19 cells were treated with TNF- α (50 ng/ml) for 24 h. (B) The conditioned medium was collected and subjected to gelatin zymography to determine the MMP-9 activity. (C) The remaining cells were lysed to assess MMP-9 protein expression by Western blotting. (D) After 6 h of TNF- α treatment in the presence or absence of LB53, ARPE-19 cell lysates were analyzed for MMP-9 mRNA by RT-PCR. The analysis was conducted from three independent results and presented as the mean \pm S.D. ### p < 0.001 compared with the resting group; * p < 0.05, ** p < 0.01, and *** p < 0.001 compared with the vehicle group stimulated with TNF- α .

cells (3×10^5 cells/ml) were seeded in 12-well plates and incubated with a stimulator (TNF- α or LPS) in the presence or absence of LB53 for 22.5 h. MTT was added (final concentration of 0.55 mg/ml) and incubated for an additional 1.5 h. Cells were then lysed with DMSO to release the purple color. The absorbance was measured by a Thermo Multiskan GO microplate reader at 550 nm (Ratastie, Finland).

2.5. Western blot analysis

Western blotting was used to detect iNOS, COX-2, MMP-9, and phosphorylated molecules in ARPE-19 and BV-2 cell lysates as previously described [30]. The protein level was quantified by optical density and expressed as the ratio: target protein/housekeeping protein (α -tubulin) or corresponding nonphosphorylated protein.

2.6. Reverse transcription-polymerase chain reaction (RT-PCR)

RNA was extracted from ARPE-19 cells by TRIreagent™ reagent, and 0.5 μ g of RNA was reverse-transcribed to cDNA and amplified according to the manual. Primers (0.2 μ M) used: human MMP-9 forward: 5'-TGG TCC TCG CCC TGA ACC TGA G-3', reverse: 5'-CGT CCA CCG GAC TCA AAG GCA C-3'; and human GAPDH forward: 5'-CCA CCC ATG GCA AAT TCC ATG GCA-3', reverse: 5'-TCT AGA CGG CAG GTC AGG TCC ACC-3'. The PCR products were then electrophoresed in a 1.5 % agarose gel and visualized by GelRed™ staining.

2.7. Nitric oxide (NO) measurement

Nitric oxide (NO) production in BV-2 conditioned medium was

measured by a nitrate/nitrite colorimetric assay kit. BV-2 cells were seeded at a density of 3×10^5 cells/ml in 12-well plates. After LB53 and/or LPS stimulation (150 ng/ml) for 24 h, the conditioned medium was collected for NO detection. Then, 100 μ l medium was mixed with 50 μ l Griess reagent A and 50 μ l Griess reagent B, followed by a 20-minute reaction. Absorbance values were measured at 550 nm by a Thermo Multiskan GO microplate reader (Ratastie, Finland). Nitrite concentrations were calculated according to the standard curve.

2.8. Measurement of reactive oxygen stress

BV-2 cells were seeded at a density of 3×10^5 cells/ml in 12-well plates. After LB53 and/or LPS stimulation (150 ng/ml) for 24 h, BV-2 cells were incubated with 2',7'-dichlorodihydrofluorescein diacetate (DCFH-DA) (10 μ M) for 40 min. Intracellular reactive oxygen species (ROS) stress was then evaluated by detecting the fluorescent intensity of 2',7'-dichlorodihydrofluorescein (DCF), the oxidized product of DCFH-DA, using flow cytometry [27].

2.9. Animals and a NaIO₃-induced AMD model

Male C57BL/6 mice (8 weeks old) were obtained from BioLASCO Taiwan Co., Ltd. (Taipei, Taiwan). Animals were maintained on a 12-hour light/dark cycle at 25 ± 1 °C and 39–45 % relative humidity. All animal experiments were performed in accordance with the Association for Research in Vision and Ophthalmology (ARVO) guidelines for ophthalmic and vision research.

Sodium iodate (NaIO₃), delivered via either intraperitoneal (i.p.) or intraocular injection, selectively induces RPE dystrophies and secondary photoreceptor degeneration, mimicking the progression and advanced features of AMD [31]. In this study, C57BL/6 mice received 25 mg/kg NaIO₃ by i.p. injection at Day 0, and LB53 (75 mg/kg) was delivered by i.p. injection 1 day before (Day -1) and 1 day after (Day 1) NaIO₃ administration. LB53 was dissolved in customized cosolvent (ethanol: cremophor:saline= 1:1:8) and given to mice once a day. Mice in the control group also received cosolvent by i.p. injection to observe possible toxicity.

2.10. Electroretinography (ERG) analysis

The retinal function of the experimental animals was evaluated using the Celeris system (Diagnosys LLC; Lowell, MA). Mice were dark-adapted overnight, and all operations were performed under dim red light on the day of ERG testing. Mice were anesthetized with a mixture of Zoletil 50™ and xylazine by i.p. injection. Mouse pupils were dilated with tropicamide (1 %) (Alcon; Geneva, Switzerland), and the eyes were instilled with Systane gel (0.3 % Hypromellose) (Alcon; Geneva, Switzerland) to keep them hydrated. As RPE is the main source of c-wave ERG responses, the preset c-wave protocol in the system was used to detect RPE activity. Recordings were obtained using 100-msec flash stimuli at an intensity of 150 cd/m², and a prolonged length of the acquisition sweep to 2–4 sec was required to detect the c-wave. In addition to the c-wave response, the protocol records the a- and b-waves, which reflect the conditions of photoreceptors and bipolar cells, respectively [32]. Amplitude (intensity) and implicit time (temporal properties) are two critical indicators for ERG responses. The amplitudes of the ERG a- and c-waves were measured from baseline to their peak, while the b-wave amplitude was measured from the preceding trough to the b-wave peak. The implicit time of ERG response was defined by the time-to-peak, measured from stimulus onset [32].

2.11. Spectral-domain optical coherence tomography (SD-OCT) imaging

The Micron III intraocular imaging system (Phoenix Research Labs, Pleasanton, CA), consisting of an OCT engine and a scanning lens, was used to detect cross-sectional tomographic images of the retina [33]. The

OCT method can monitor retinal morphology in living animals without invasive surgery. OCT results were imported into InSight XL software (Phoenix Research Laboratories) to measure the specific and total retinal thickness.

2.12. Measurement of retinal blood flow by laser speckle flowgraphy (LSFG)

Retinal blood flow was evaluated by the noninvasive LSFG-Micro system (Softcare Co., Ltd.; Fukuoka, Japan). The system uses a diode laser (wavelength 830 nm) equipped with an ordinary charge-coupled camera (output image resolution 700 × 480 pixels). Blood flow was measured in mice 7 min after the induction of anesthesia by i.p. injection of a mixture of Zoletil 50™ and xylazine. To produce a temporal composite, images were captured continuously at a rate of 30 FPS over 4 seconds. A representative color map was acquired and analyzed by LSFG Analyzer software (version 3.5.0.0; Softcare, Co., Ltd.). The results were quantified as mean blur rate (MBR), an indicator of the relative velocity of red blood cell movement to reflect blood flow rate. Red indicates faster blood flow, while blue indicates a slower speed.

2.13. Statistical analysis

The experimental results were analyzed by GraphPad Prism 7.00 software. One- or two-way analysis of variance (ANOVA) with the Newman-Keuls test was used to calculate statistical significance. The data shown on the histogram are expressed as the mean \pm S.D. A p value < 0.05 was considered statistically significant.

3. Results

3.1. LB53 attenuated TNF- α -induced MMP-9 expression and activities in ARPE-19 cells

To assess whether LB53 treatment reduced MMP-9 expression, the proinflammatory cytokine TNF- α was applied to ARPE-19 cells, as proteome profiling revealed that extracellular matrix remodeling-related proteins, including MMP-9, were more abundant in TNF- α -treated ARPE-19 cells [34]. Cell viability of ARPE-19 was first tested after LB53 (2, 5, 10, and 20 μ M) treatment (Fig. S1A). LB53 alone didn't obviously affect cell viability even at highest concentration (20 μ M). After TNF- α stimulation in the presence or absence of LB53 (2, 5, 10, and 20 μ M) in ARPE-19 (Fig. S1B), we found that high concentration of LB53 (20 μ M) led to decreased cell viability (34.95 ± 3.90 %). LB53 concentrations within the range of 2–10 μ M were therefore used for the following *in vitro* study on ARPE-19 cells. As shown in Fig. 1B, the gelatin zymography results showed that MMP-9 activity was significantly induced by 50 ng/ml TNF- α (vehicle group; 2.68 ± 0.49 -fold) compared with the resting group. LB53 concentration-dependently attenuated TNF- α -induced gelatinization activity of MMP-9 (LB53 2 μ M: 2.17 ± 0.40 -fold; 5 μ M: 1.69 ± 0.11 -fold; 10 μ M: 1.25 ± 0.31 -fold). Consistent with the results, LB53 transcriptionally repressed MMP-9 protein and mRNA expression in a concentration-dependent manner in TNF- α -stimulated ARPE-19 cells (Figs. 1C and 1D). LB53 suppressed MMP-9 protein at 2 μ M (2.52 ± 0.24 -fold), 5 μ M (2.15 ± 0.14 -fold), and 10 μ M (1.58 ± 0.13 -fold) compared to the vehicle group (3.55 ± 0.51 -fold) (Fig. 1C). MMP-9 mRNA was decreased by LB53 at 2 μ M (4.64 ± 0.55 -fold), 5 μ M (4.09 ± 0.41 -fold), and 10 μ M (2.97 ± 0.51 -fold) compared to the vehicle group (5.06 ± 0.70 -fold) (Fig. 1D).

3.2. LB53-mediated MMP-9 inhibition via NF- κ B signaling in ARPE-19 cells

Inflammation caused by proinflammatory stimuli such as TNF- α depends on the activation of NF- κ B [35]; therefore, we investigated the role of NF- κ B in MMP-9 expression in TNF- α -stimulated ARPE-19 cells.

Phosphorylation of p65 peaked at 5 min after TNF- α stimulation (Fig. S2) (1.56 \pm 0.16-fold) compared with 15 min (1.21 \pm 0.20-fold), 30 min (1.12 \pm 0.10-fold), and 45 min (0.75 \pm 0.08-fold). LB53 concentration-dependently suppressed p65 phosphorylation after 5 min of TNF- α stimulation (Fig. 2A). The release of p65 is associated with multiple mechanisms, including the activation of IKK α/β and the degradation of I κ B inhibitor proteins [35,36]. After TNF- α stimulation, LB53 reduced IKK α/β phosphorylation (Fig. 2B) and reversed I κ B degradation (Fig. 2C) in a concentration-dependent manner. In addition, PI3K, p38, and JNK signaling pathways, especially p38 signaling, have been found to be involved in MMP-9-evoked human RPE responses [37]. Thus, we examined whether LB53 inhibits p38 activity in TNF- α -stimulated ARPE-19 cells. TNF- α significantly induced the phosphorylation of p38 (1.66 \pm 0.24-fold), and LB53 did not affect p38 activation at the indicated concentrations (Fig. 2D).

3.3. LB53 attenuated microglia-produced inflammatory mediators via NF- κ B signaling

The histopathological retina of AMD revealed that microglia accumulated near the drusen deposits [22] and produced a variety of inflammatory mediators that promote disruption of Bruch's membrane and progression of AMD [38]. We next examined the anti-inflammatory effects of LB53 in LPS-stimulated BV-2 microglia. LPS is a Toll-like receptor 4 (TLR4) activator, and during retinal degeneration, microglia can be activated through the TLR4 pathway [39,40]. LPS (150 ng/ml) significantly induced the expression of the inflammatory mediators iNOS (34.52 \pm 4.12-fold) and COX-2 (28.91 \pm 4.92-fold) compared to the resting conditions in BV-2 microglial cells (Figs. 3A and B). Treatment with LB53 concentration-dependently inhibited LPS-activated iNOS (2 μ M: 27.82 \pm 1.36-fold; 5 μ M: 16.74 \pm 1.4-fold; 10 μ M: 7.74 \pm 3.26-fold) and COX-2 protein expression (2 μ M: 25.54 \pm 5.18-fold; 5 μ M: 21.11 \pm 4.71-fold; 10 μ M: 15.65 \pm 3.89-fold) compared to vehicle (Fig. 3A and B). BV-2 microglia were tested for cell viability after

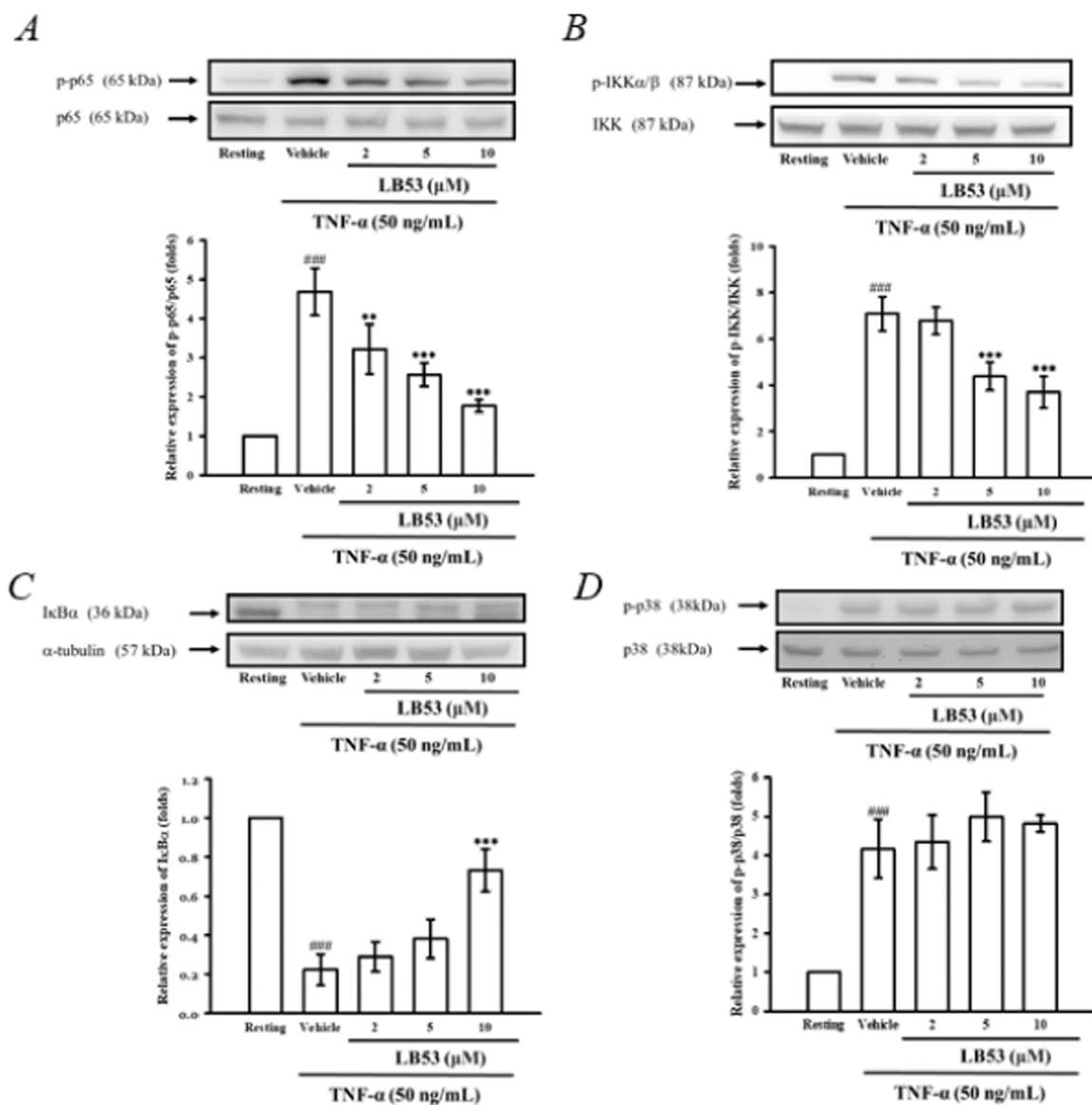
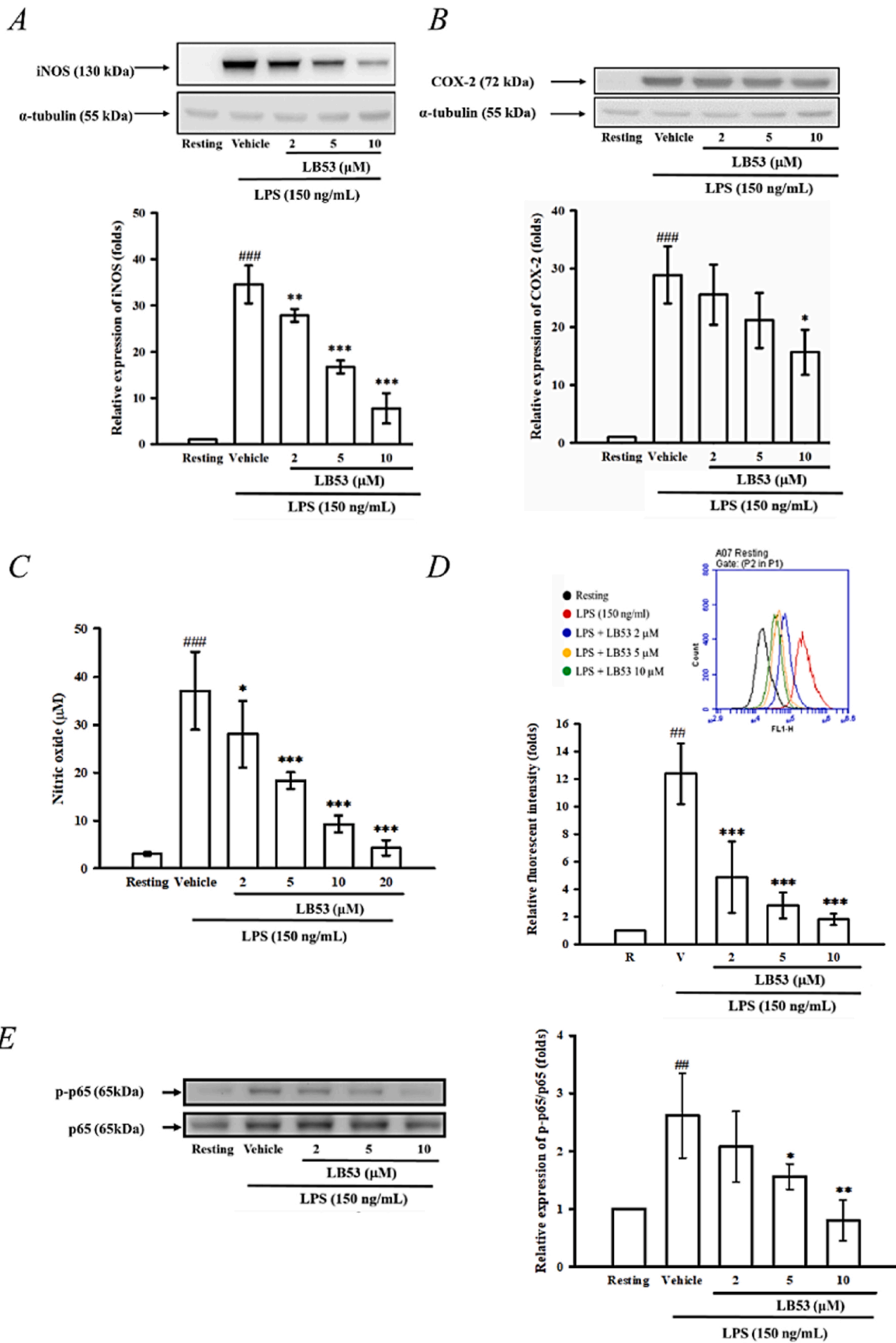


Fig. 2. Signalings of LB53 on TNF- α -stimulated ARPE-19 cells. ARPE-19 cells (1×10^6 cells/ml) were seeded in 6-well plates. Cells were pretreated with LB53 (2, 5 and 10 μ M) or vehicle for 30 min followed by TNF- α (50 ng/ml) stimulation for the indicated period (p65 and IKK: 5 min; I κ B and p38: 30 min). The cell lysates were analyzed for phosphorylation of (A) p65, (B) IKK, (D) p38 and (C) protein degradation of I κ B α by Western blots. Three independent experiments were analyzed and are presented as the mean \pm S.D. ###p < 0.001 compared with the resting group; * *p < 0.01 and * * *p < 0.001 compared with the vehicle (DMSO) group.



(caption on next page)

Fig. 3. Effects of LB53 on LPS-induced inflammatory responses and reactive oxygen stress in microglial BV-2 cells. BV-2 cells (3×10^5 cells/ml) were seeded in 12-well plates. After treatment with LB53 (2, 5, 10 and/or 20 μ M) or vehicle for 30 min, BV-2 cells were stimulated with LPS (150 ng/ml) for 24 h. The cell lysates were subjected to Western blotting to detect (A) iNOS and (B) COX-2 protein expression. (C) The conditioned medium was collected and assayed for nitric oxide levels. (D) Twenty-four hours post-LPS stimulation, BV-2 microglial cells were incubated with DCFH-DA (10 μ M) for 40 min. Cells were then trypsinized and analyzed for DCF fluorescence intensities to evaluate reactive oxygen stress levels by flow cytometry. (E) BV-2 cells (1×10^6 cells/ml) were seeded in 6-well plates and treated with LPS (150 ng/ml) in the presence or absence of LB53 (2, 5 and 10 μ M) or vehicle. The cell lysates were analyzed for phosphorylation of p65 protein by Western blots. Three independent results were used for analysis and are expressed as the mean \pm S.D. $^{##}p < 0.01$ and $^{###}p < 0.001$ compared with the resting group; $^*p < 0.05$, $^{**}p < 0.01$, and $^{***}p < 0.001$ compared with the LPS-treated vehicle group (DMSO).

LB53 (5, 10, and 20 μ M) and/or LPS treatment (Fig. S1C). High concentration of LB53 (20 μ M) combined with LPS resulted in decreased cell viability (73.39 ± 0.99 % compared with 100 % in the resting group),

whereas LPS alone or LPS combined with LB53 at 5 and 10 μ M did not affect cell viability (5 μ M: 97.10 ± 12.38 %; 10 μ M: 89.81 ± 9.83 %) (Fig. S1C). Compared with the resting group, LPS significantly elicited

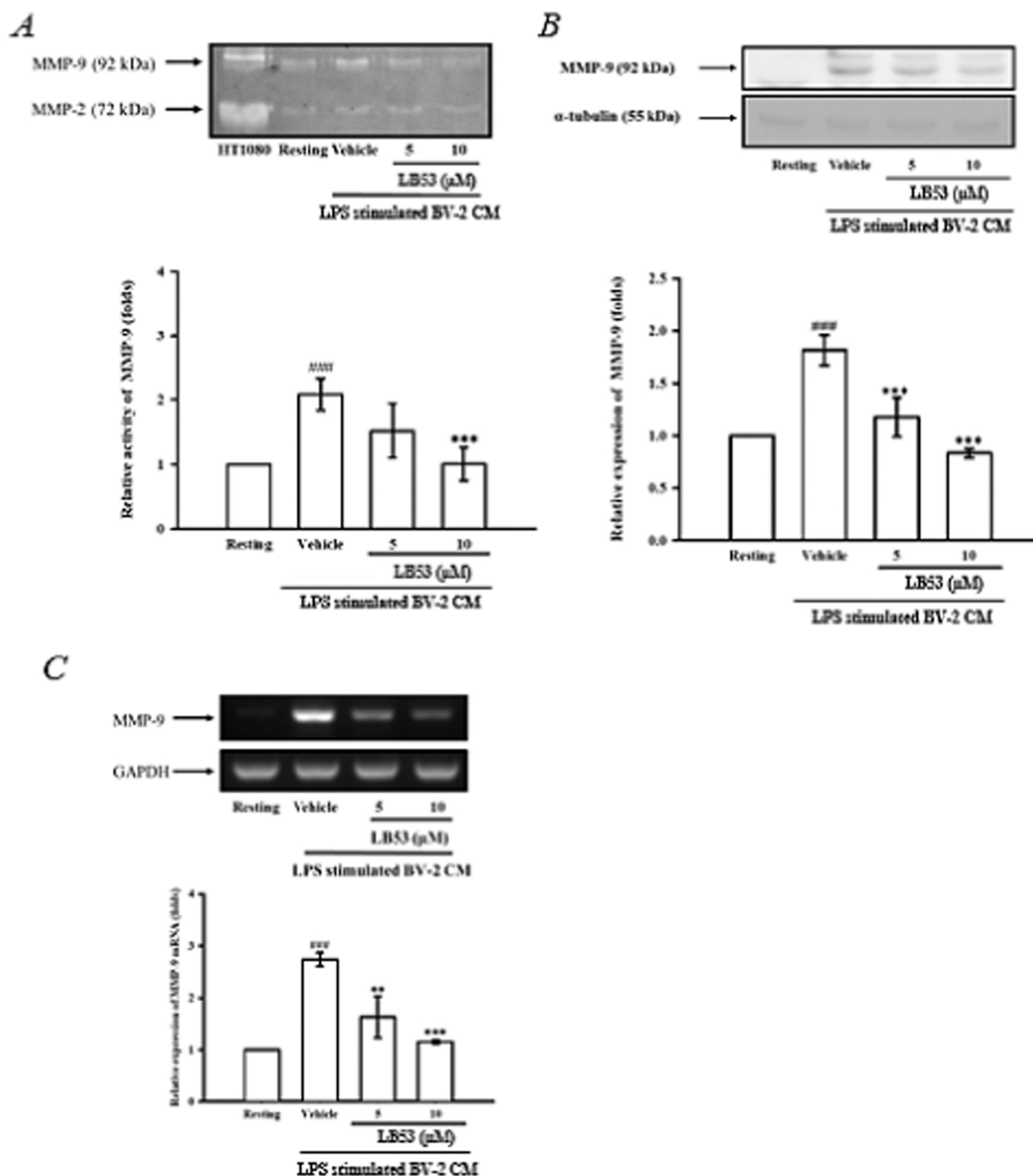


Fig. 4. Effects of LB53 on ARPE-19 MMP-9 activation induced by LPS-stimulated BV-2 conditioned medium. BV-2 cells (3×10^5 cells/ml) were seeded in 12-well plates and treated with LPS (150 ng/ml) for 24 h. The conditioned medium (CM) from LPS-stimulated BV-2 cells was collected. ARPE-19 cells were pretreated with LB53 (5 and 10 μ M) for 30 min followed by exposure to the aforementioned CM for 24 h. (A) The conditioned medium from ARPE-19 cells was then subjected to gelatin zymography to detect MMP-9 activity. (B) Cell lysates were detected for MMP-9 protein levels by Western blotting. (C) After treatment with CM from LPS-stimulated BV2 cells, the ARPE-19 cells were evaluated for MMP-9 mRNA expression by RT-PCR. Three independent experiments were analyzed and conducted as the mean S.D. $^{###}p < 0.001$ compared with the resting group; $^{**}p < 0.01$ and $^{***}p < 0.001$ compared with the vehicle (DMSO).

reactive nitric oxide levels (37.08 ± 8.51 -fold) (Fig. 3C), and LB53 significantly reduced the nitric oxide level (2 μ M: 28.07 ± 6.96 -fold; 5 μ M: 18.35 ± 1.76 -fold; 10 μ M: 9.26 ± 1.75 -fold) in the vehicle group (Fig. 3C). Microglia are considered to be a major source of oxidative stress in the eye [41]. In BV-2 microglia, LPS triggered intracellular reactive oxygen species (ROS) labeled by DCF fluorescence by 12.9 ± 2.2 -fold compared with resting conditions (Fig. 3D). LC53 treatment concentration-dependently suppressed ROS production (2 μ M: 4.9 ± 1.5 -fold; 5 μ M: 2.8 ± 0.5 -fold; 10 μ M: 1.8 ± 0.4 -fold). Since LPS activation of TLR4 leads to a series of signaling cascades that lead to NF- κ B activation and the release of proinflammatory cytokines [42], we

assessed the inhibitory effect of LB53 on p65 activation upon LPS stimulation. LB53 suppressed LPS-induced p65 phosphorylation (2.62 ± 0.41 -fold) in a concentration-dependent manner (2 μ M: 2.09 ± 0.44 -fold; 5 μ M: 1.93 ± 0.15 -fold; 10 μ M: 0.91 ± 0.03 -fold) (Fig. 3E).

3.4. LB53 inhibited MMP-9 expression in the inflammation-activated BV-2 microglial supernatant-activated RPE

The interaction of microglia and the RPE has an important role in inflammation in AMD [7,43]. Microglia trigger a more proinflammatory, chemoattractive, and proangiogenic environment by

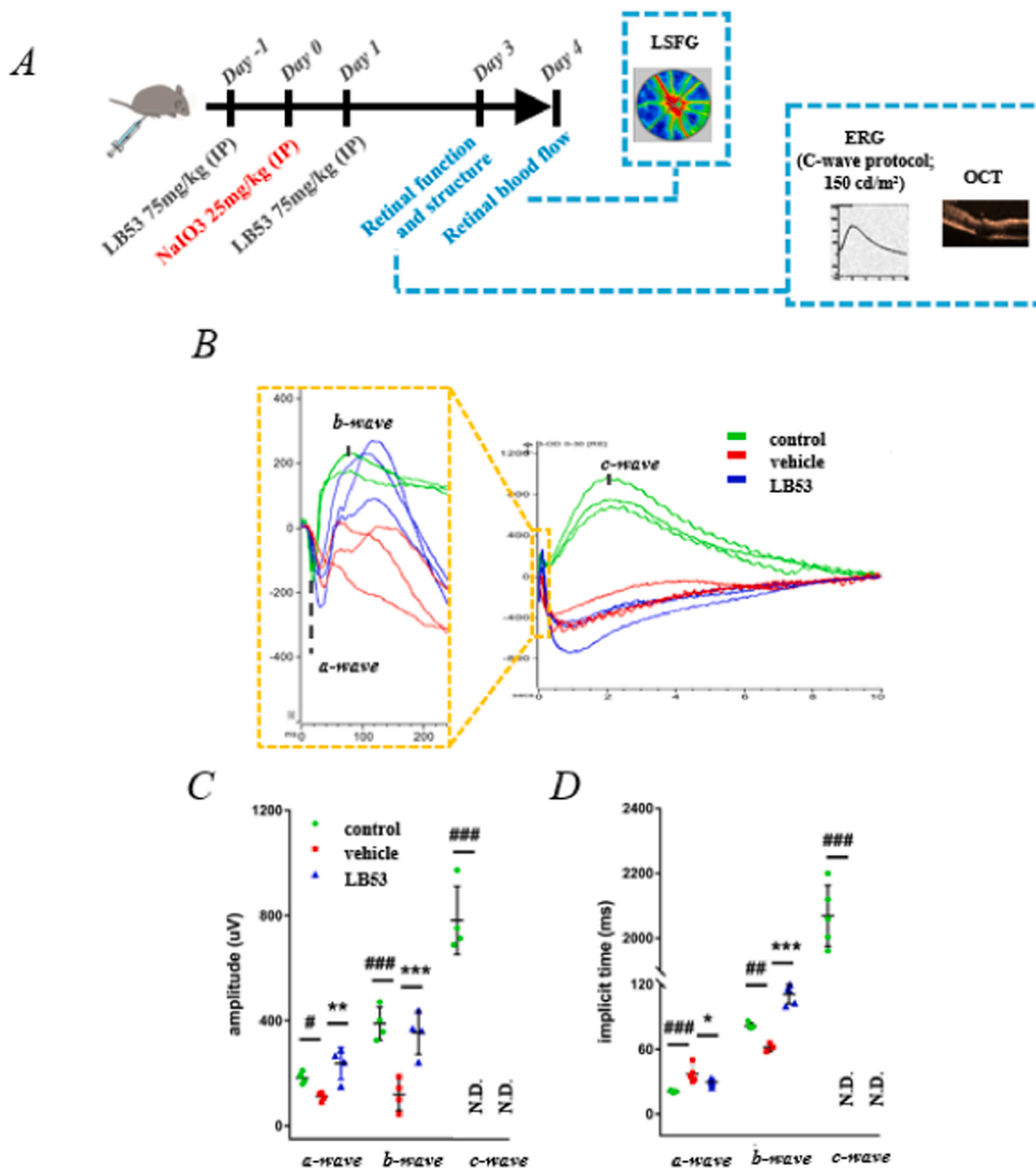


Fig. 5. Effects of LB53 on the NaIO₃-induced retinal function degeneration. (A) Schematic illustration of the NaIO₃-induced mouse model of retinal degeneration and the LB53 regimen. (B) ERG responses (C-wave protocol) from control mice (green curve) and mice treated with vehicle (red curve) or LB53 (blue curve) were recorded 3 days after NaIO₃ injection. Three representative responses shown from each group were acquired from 3 independent animals. The inset shows a high-magnification image of the selected area (orange dotted box) to illustrate the a- and b-waves. (C, D) Quantification of the average amplitudes and implicit time (time to peak) from 3 to 5 animals per group. The ERG a-waves were negative, and the a-wave amplitudes are presented as the absolute value. The data are presented as the mean \pm S.D. IP, intraperitoneal; OCT, optical coherence tomography; LSFG, laser speckle flowgraphy; ERG, electroretinography. # $p < 0.05$, ## $p < 0.01$, and ### $p < 0.001$ compared with the control; * $p < 0.01$ and ** $p < 0.001$ compared with the NaIO₃-injured vehicle group. N.D., not detected.

altering the RPE during AMD [24]. We next investigated the interaction of activated microglial BV-2 cells with RPE. Conditioned medium from LPS-stimulated BV-2 microglia caused 2.09 ± 0.25 -fold and 1.87 ± 0.23 -fold greater MMP-9 activation and protein expression in RPE compared to the resting group, respectively (Fig. 4A and B). LB53 treatment suppressed MMP-9 activation (5 μ M: 1.52 ± 0.42 -fold; 10 μ M: 1.01 ± 0.25 -fold) and protein expression (5 μ M: 1.27 ± 0.29 -fold; 10 μ M: 0.99 ± 0.18 -fold) in a concentration-dependent

manner (Fig. 4A and B). We were unable to detect MMP-9 gelatinase activity by zymography in LPS-stimulated BV-2 microglia (data not shown). Furthermore, LB53 (5 and 10 μ M) inhibited MMP-9 mRNA expression in activated RPE cells (Fig. 4C).

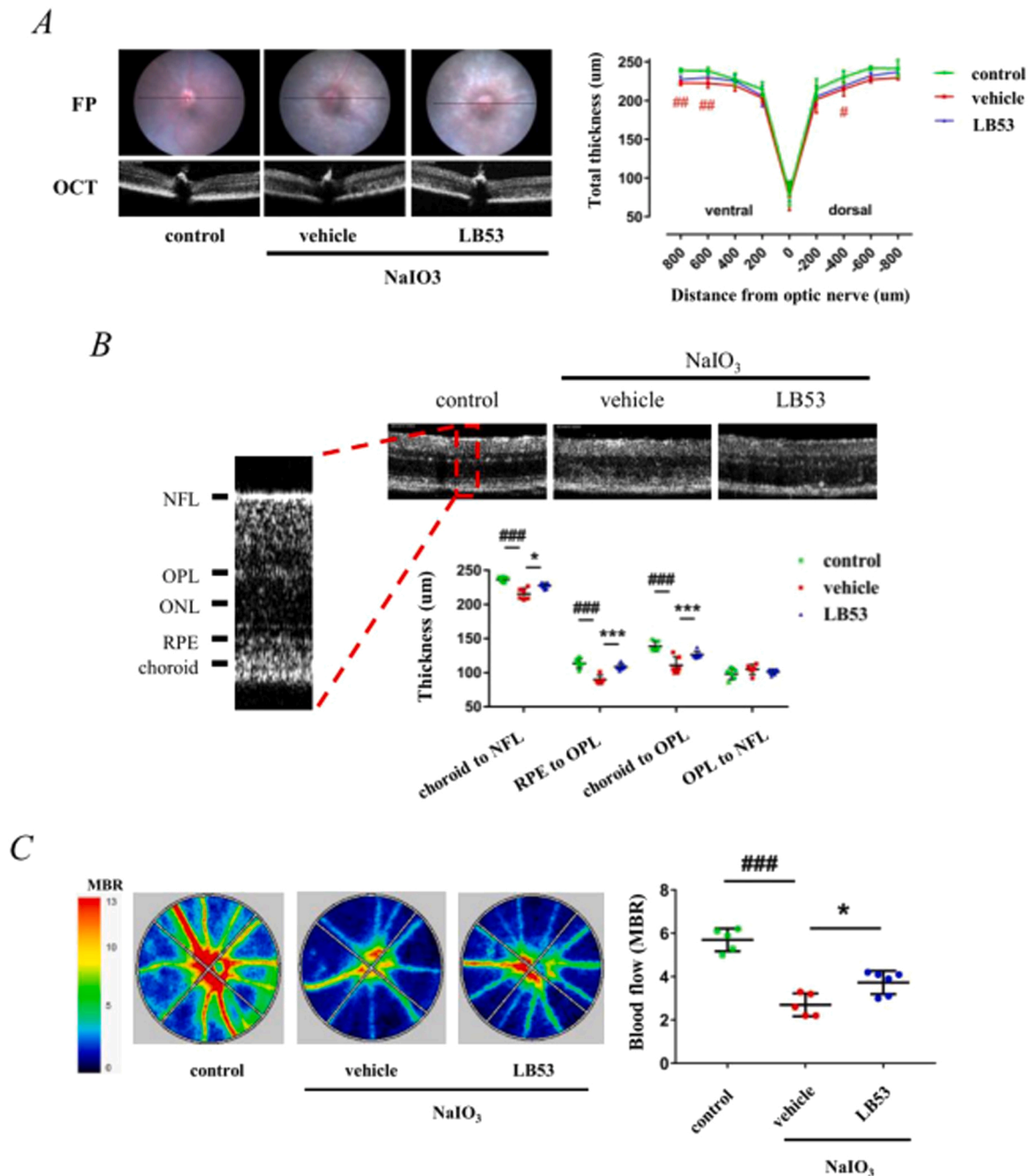


Fig. 6. Regulation of retina structure and blood flow by LB53 in NaIO₃-induced retinal degeneration. (A) Toggles labeled on FP are representative of the OCT scanning area. The total retina thickness measured from OCT sections at 200 μ m intervals was plotted versus the distance from the optic nerve (n = 4–6 each group). (B) High-magnification OCT images captured at approximately 500 μ m from the optic nerve were quantified for the thickness of the separated retina layer using InSight XL software (n = 6 each group). (C) A representative color-coded map of retinal blood flow was imaged by laser speckle flowgraphy (LSFG). LSFG results were analyzed and expressed as the mean blur rate (MBR), an index for the relative velocity of erythrocyte movement, indicating the blood flow rate. Red color indicates faster blood flow, while blue color indicates slower blood flow. Four quadrants annotated in Fig. 6C were analyzed for the MBR value by LSFG Analyzer software. (n = 5–6 each group). The data are presented as the mean \pm S.D. FP, fundus photography; NFL, nerve fiber layer; OCT, optical coherence tomography; ONL: outer nuclear layer; OPL: outer plexiform layer; RPE: retinal pigment epithelium; MBR, mean blur rate. ###p < 0.001 compared with the control; *p < 0.05 and **p < 0.001 compared with the vehicle-treated NaIO₃-injured group.

3.5. LB53 protected mice from NaIO₃-induced functional degeneration in the retina

To assess whether LB53 treatment preserves the degeneration of RPE or retinal cells *in vivo*, a sodium iodate (NaIO₃)-induced mouse model of retinal degeneration that features dry AMD was applied [31]. The experimental design is shown in Fig. 5A. C57BL/6 mice received 25 mg/kg NaIO₃ by i.p. injection at Day 0. LB53 (75 mg/kg) was intraperitoneally injected 1 day before (Day -1) and 1 day after (Day 1) NaIO₃ administration. Retinal function and structure were evaluated 3 days post-NaIO₃ administration by electroretinography (ERG) and optical coherence tomography (OCT), respectively. Retinal circulation (blood flow) was measured by laser speckle flowgraphy (LSFG) 4 days after NaIO₃ administration. To examine retinal function, we measured ERG using a c-wave protocol in LB53- and/or NaIO₃-treated mice. A dark-adapted c-wave protocol records a, b, and c-waves, which are derived from rod photoreceptors (nuclear location in the outer nuclear layer (ONL)), bipolar cells, and retinal pigment epithelium (RPE) [32]. Compared with the control group, NaIO₃ caused a decline in the C-wave response (Fig. 5B) and thus undetectable amplitude (Fig. 5C) and implicit time (5D), suggesting RPE dystrophy-related loss of functional. Administration of LB53 did not protect against NaIO₃-induced RPE dysfunction (loss of c-wave response) in mice (Fig. 5B - D), which is consistent with our *in vitro* data that LB53 did not rescue NaIO₃-elicited ARPE-19 cell death (Fig. S1D). Rod photoreceptors are the primary source for the a-wave response. NaIO₃ treatment affected rod photoreceptors, resulting in a reduced a-wave amplitude ($112.0 \pm 16.3 \mu\text{V}$) and prolonged implicit time ($37.0 \pm 7.9 \text{ msec}$) compared to the control group (amplitude: $183.0 \pm 23.1 \mu\text{V}$; implicit time: $21.0 \pm 0.7 \text{ msec}$). LB53 rescued the functions of amplitude ($238.0 \pm 60.7 \mu\text{V}$) and implicit time ($29.6 \pm 3.2 \text{ msec}$) (Fig. 5B - D). NaIO₃ administration significantly impaired bipolar cell functions by reducing the b-wave amplitude ($119.0 \pm 60.8 \mu\text{V}$) and shortening implicit time ($62.0 \pm 4.0 \text{ msec}$) compared with the control group (amplitude: $390.0 \pm 62.9 \mu\text{V}$; implicit time: $81.6 \pm 2.5 \text{ msec}$). LB53 significantly prevented NaIO₃-induced loss of b-wave response by restoring the amplitude ($354.0 \pm 81.9 \mu\text{V}$) and implicit time ($111.0 \pm 8.9 \text{ msec}$) (Fig. 5B - D). We repeated the experiment shown in Fig. 5A but without NaIO₃ administration to test the side effects of LB53, and we didn't find adverse effects on ocular surface, the fundus, retinal structure (detected by OCT) (Fig. S3A), and also the retinal functions (assayed by ERG) from LB53 alone treatment compared with control group. (Fig. S3B).

3.6. LB53 preserved retina structure and regulated blood flow in NaIO₃-injured retinas

Representative fundus photography (FP) showed that some pale plaques around the fundus after exposure to NaIO₃ on Day 3 (Fig. 6A), which may be related to the altered opacity caused by atrophy of the scattered RPE. Total retinal thickness was analyzed from OCT images and plotted every 200 μm intervals beginning from the optic nerve to the ventral and dorsal directions along the vertical axis (Fig. 6A). Three days of NaIO₃ exposure resulted in retinal thinning, and LB53 administration mildly protected the effect (Fig. 6A). Although retinal thinning was not dramatically observed after NaIO₃ treatment, outer retinal disorganization (RPE to OPL) was more frequently observed than the inner retina according to magnified OCT images (scanning at approximately 500 μm away from the optic nerve) (Fig. 6B). NaIO₃ caused significant thickness reductions in the choroid to nerve fiber layer (NFL) ($215.5 \pm 8.1 \mu\text{m}$), RPE to OPL ($89.8 \pm 6.6 \mu\text{m}$), and choroid to OPL ($110.8 \pm 12.5 \mu\text{m}$) but not in the OPL to NFL ($104.7 \pm 7.1 \mu\text{m}$) compared to controls (choroid to NFL, $236.6 \pm 4.1 \mu\text{m}$; RPE to OPL, $113.5 \pm 7.0 \mu\text{m}$; choroid to OPL, $138.5 \pm 7.2 \mu\text{m}$; and OPL to NFL, $98.2 \pm 8.1 \mu\text{m}$, respectively). LB53 treatment preserved the outer retinal thickness, mainly in the ONL and mildly in the RPE and choroid layer, after NaIO₃ exposure (choroid to NFL, $227.6 \pm 4.2 \mu\text{m}$; RPE to OPL, $108.6 \pm 4.4 \mu\text{m}$; choroid to OPL,

$126.4 \pm 5.1 \mu\text{m}$; and OPL to NFL, $101.2 \pm 3.8 \mu\text{m}$, respectively).

Similar to AMD pathology, decreased retinal blood flow occurred after NaIO₃-induced RPE atrophy [44]. In this context, the LSFG-Micro system was used to examine the retinal blood flow in NaIO₃-injured mouse retinas. LSFG results were generated from the representative colormap shown in Fig. 6C and expressed as mean blur rate (MBR). After 4 days of NaIO₃ exposure, the mean MBR value in the four annotated quadrants decreased to 2.7 ± 0.5 compared to 5.7 ± 0.5 in the control group, and LB53 treatment significantly restored the blood flow in the retina by 3.7 ± 0.5 .

4. Discussion

The etiology of AMD is closely related to chronic inflammation, which involves neuroinflammation, ECM turnover, growth factor imbalance, oxidative stress, and complement activation [19,45]. Matrix metalloproteinases (MMPs) have multiple roles in these processes, and MMPs secreted by RPE have been shown to contribute to the pathogenesis of AMD [9,10,19,46]. Retinal microglia are also a known source of MMPs in the AMD models, but more attention has been focused on their classic role in neuroinflammation [8]. This study reveals that theissenolactone B (LB53), a fungal-derived natural compound, displays strong anti-MMP-9 activities in RPE cells and an anti-inflammatory response in microglia *in vitro*. Although LB53 did not restore RPE functional loss or disorganization, it significantly preserved retinal neuronal function (photoreceptors and bipolar cells) and improved retinal blood flow in NaIO₃-induced retinal degeneration.

MMP activity is physiologically required for tissue remodeling, primarily through cleavage of extracellular matrix or protein substrate, but alterations in MMP activities have been widely reported in AMD. Previous studies reported that MMP-2, MMP-3, and MMP-9 were found in human RPE-Bruch's membrane, stroma, and vessels, and the levels of two gelatinases, MMP-2 and MMP-9, were increased with donor age [10, 16]. In addition to their incremental changes observed in human specimens, MMP-2 and MMP-9 preferentially catalyze collagen type IV, which is a key component of the basement surrounding vessels, Bruch's membrane, and ECM [47,48]; thus, special attention has been given to these two MMPs in AMD.

Bruch's membrane is arranged between the RPE and the choroid with a distinct five-layer structure. The RPE basement membrane is located on the apical side, and the choriocapillary basement membrane is located on the basal side [49]. MMP-9 mediates epithelial barrier disruption in the RPE by affecting occludin and ZO-1, and proteolysis of the endothelial basement membrane allows the influx of circulating leukocytes and plasma protein into the immune-privileged retina [9,50], triggering an inflammatory stimulus in tissue injury. MMP-2 and MMP-9 activate pro-inflammatory cytokines, such as IL-8, IL-1 β , and TNF- α , by truncating their full-length forms [50,51]. In addition, increased cleavage of cell-surface FasL by MMPs results in restricted apoptosis of infiltrated leukocytes [52]. Continued infiltration of immune cells and the presence of proinflammatory mediators in the retina thus lead to chronic inflammation, accelerating the progression of dry AMD. Regarding wet AMD, the role of MMP-9 in CNV progression has also been explained [8,15,19]. Since MMP-9 is closely associated with AMD disease, and RPE is a major source of this enzyme [46], we tested the anti-MMP-9 activities of LB53 in the TNF- α -stimulated human ARPE-19 cell line. Gelatin zymography assays revealed that TNF- α substantially elicited MMP-9 activation in ARPE-19 cells, but not MMP-2. MMP-2 was consistently activated, regardless of TNF- α treatment (Fig. 1B). TNF- α also stimulated MMP-9 mRNA and protein expression in ARPE-19 cells (Fig. 1C, D). LB53 significantly inhibited the activation of MMP-9 and its transcription upon TNF- α stimulation, suggesting that LB53 has a strong pharmacologic effect against MMP-9 (Fig. 1B - D).

In the RPE, the signaling pathway of TNF- α -induced MMP-9 has been extensively investigated. The natural compound quercetin inhibits TNF- α -induced MMP-9 and ICAM-1 expression in ARPE-19 cells via the

MAPK and NF- κ B pathways [36]. Wang et al. reported that TNF- α promotes MMP-9 expression by activating Akt/mTORC1 but not MAPK signaling, thereby enhancing RPE cell migration [53]. LB53 significantly attenuated signaling axes that synergize with canonical NF- κ B signaling [35] in TNF- α -stimulated ARPE-19 cells, including phosphorylation of IKK α/β , degradation of I κ B, and phosphorylation of p65 (Fig. 2A - C). We also detected MAPK p38 activity in this cellular model, whereas LB53 did not affect TNF- α -elicited p38 activation (Fig. 2D). The genes encoding complement C3, syndercan-4, and plasminogen activator inhibitor related to pathogenesis of AMD all have NF- κ B binding site in their promoter regions. Application of LB53 may reduce the synthesis of these mediators in the AMD retinas in response to TNF- α exposure [34].

In addition to RPE-mediated MMP9 activities, the inflammatory responses by resident microglia also contribute to pathogenesis of AMD [54]. Retinal microglia are normally absent from the outer retina. In cases of advanced disease, the disruption of the RPE epithelial barrier allows the recruitment of microglia and inflammatory cells into the locus of AMD, creating an inflammatory microenvironment by the release of proinflammatory cytokines [24]. VEGF is the primary proangiogenic factor that promotes CNV secondary to dry AMD, and proinflammatory cytokines, including IL-1 β , IL-6 and TNF- α , may exacerbate neuronal damage. In addition, increased production of MIP-2 and MCP-1 amplifies the inflammatory chemoattractant [43]. Toll-like receptor 4 (TLR4) is critical for microglial activation in many neuroinflammatory and retinal degenerative diseases [40,55]. The immune-driven mediators, including inducible NO synthase (iNOS) and cyclooxygenase-2 (COX-2), are induced under inflammatory conditions, leading to the production of cytotoxic NO and proinflammatory prostaglandins, respectively [56]. We next tested the anti-inflammatory activities of LB53 in BV-2 microglia for iNOS and COX2 production after stimulation with a known TLR4 agonist, lipopolysaccharide (LPS) [56]. LPS strongly induced iNOS, COX-2, and NO production in BV-2 cells, whereas LB53 showed strong inhibition of iNOS and downstream NO production, but mild inhibition on COX-2 (Fig. 3A - C). Along with NO species, microglia are also considered to be a main source of reactive oxygen species (ROS) in the eye [57]. Since oxidative stress cooperatively promotes AMD pathogenesis by promoting inflammation, angiogenesis and drusen-related protein transcripts [58,59], we evaluated the antioxidant effect of LB53 in LPS-stimulated BV-2 microglia. The DCFH-DA assay results revealed that LB53 had a significant inhibitory effect on LPS-induced ROS production in BV-2 cells (Fig. 3D). Similar to the pathway regulated in the RPE (Fig. 2A), LB53 significantly inhibited p65 activation (Fig. 3E). Given these anti-microglial activities via suppression of inflammatory responses and oxidative stress, LB53 may serve as a potential treatment for neuroinflammatory diseases, including AMD, which are affected by dysfunctional microglia.

As mentioned above, microglia are normally absent in the outer retina but migrate to the subretinal sites around the RPE-Bruch's membrane during AMD progression [24]. The interaction of activated microglia with the RPE causes multiple structural and functional deficiencies of the latter, such as the reduction of RPE65 (visual cycle protein) and tight-junctional proteins (ZO-1 and claudin-1) [20]. *In vitro* studies also revealed markedly increased gene/protein expression levels of proinflammatory cytokines (IL-1 β and TNF- α), chemotactic cytokines (MCP-1 and SDF-1), adhesion molecules (VCAM-1 and ICAM-1), and proangiogenic molecules (VEGF and MMP-1, -2, -9) in RPE exposed to activated microglia [24]. Blockade of microglia attenuated the inflammatory response, complement activation, and inflammasome formation in RPE-exposed to activated microglia [60]. In this study, conditioned medium (CM) of LPS-activated BV-2 microglial cells was used to stimulate ARPE-19 cells, and a cellular model was used to evaluate the regulation of MMP-9 expression in RPE by LB53. BV-2 CM significantly induced MMP-9 enzymatic activation, protein expression, and gene expression in ARPE-19 cells (Fig. 4A - C), consistent with other findings on inflammatory responses associated with cell-cell interactions. LB53 pretreatment effectively inhibited these effects in BV-2 CM-stimulated

ARPE-19 cells, suggesting that LB53 may potentially protect the RPE-mediated immune privileged milieu from activated microglia attack, thereby ameliorating the pathogenesis of AMD management of associated chronic neuroinflammation.

Sodium iodate (NaIO₃) directly induces RPE necroptosis, resulting in sheet-like loss of RPE with secondary effects on photoreceptors and choriocapillaris *in vivo* [61]. Due to these phenomena that feature the pathology of AMD, NaIO₃ injection has been widely used as a preclinical model for diseases characterized by extensive RPE degeneration, including advanced dry AMD or geographic atrophy (GA) [31]. In this study, an AMD model of NaIO₃-induced retinal degeneration was used to test the protective effects of LB53. Indeed, NaIO₃ degenerated the RPE as no c-wave response reflecting the RPE condition was detected (Fig. 5B). Treatment with LB53 did not preserve the RPE function from NaIO₃, which is consistent with the OCT results, showing that LB53 largely restored ONL thickness, but only slightly restored the RPE or choroid layer (Fig. 5F). The preservation of the ONL layer was found in not only the structural observation but also the functional assay given that LB53 restored the a-wave response (Fig. 5B). Interestingly, while NaIO₃ caused a clear loss of function in the b-wave response (Fig. 5B), we did not find structural degeneration in the bipolar cell layer (Fig. 5F). This may be due to an aberrant signal transduction cascade at the level of photoreceptors to depolarizing bipolar cells, rather than a direct defect in bipolar cells [62]. LB53 treatment significantly protected bipolar cell function from NaIO₃. Decreased retinal blood flow velocity has been found in patients with AMD. Clinical symptoms may be related to the loss of metabolic transport function in the RPE, resulting in impaired choroidal perfusion [63,64]. In our studies, LB53 effectively rescued the NaIO₃-impaired retinal blood flow (Fig. 6), suggesting its pharmacological role in repairing retinal vascular perfusion.

5. Conclusion

In conclusion, our findings demonstrate that LB53 is able to preserve retinal neuronal function (photoreceptors and bipolar cells) and improve retinal blood flow in NaIO₃-induced retinal degeneration model of AMD. Cellular studies indicate that LB53 had strong anti-MMP-9 activities in RPE cells and an anti-inflammatory/oxidative response in microglia. Additionally, LB53 regulates inflammatory responses associated with RPE-microglia interactions. Given its neuroprotective and immunoregulatory effects, LB53 may be a potential therapeutic agent for advanced dry AMD to delay further vision loss and prevent CNV development (wet AMD).

Funding

This work was supported by the Ministry of Science and Technology of Taiwan [grant numbers: MOST 107-2320-B-038-025-MY3 and 110-2320-B-038-036-MY3].

Ethic approval

The animal use was authorized by the Institutional Animal Care and Use Committee of Taipei Medical University [LAC-2017-0516 and LAC-2020-0495].

CRedit authorship contribution statement

Fan-Li Lin: Conceptualization, Methodology / Study design, Investigation, Data curation, Writing – original draft, Visualization, **Yu-Wen Cheng:** Conceptualization, Methodology / Study design, Resources, Writing – review & editing, Supervision, **Li-Huei Chen:** Methodology / Study design, Investigation, Data curation, Visualization, **Jau-Der Ho:** Conceptualization, Resources, Writing – review and editing, **Jing-Lun Yen:** Methodology / Study design, Investigation, Data curation, Visualization, **Mong-Heng Wang:** Methodology / Study design, Resources,

Writing – review & editing, **Tzong-Huei Lee**: Conceptualization, Methodology / Study design, Resources, Writing – review & editing, Project administration, **George Hsiao**: Conceptualization, Methodology / Study design, Data curation, Writing – review & editing, Supervision, Project administration, Funding acquisition.

Data Availability

Data will be made available on request.

Acknowledgments

The authors acknowledge the study's funders.

Competing interests

The authors declare that they have no conflicts of interest.

Appendix A. Supporting information

Supplementary data associated with this article can be found in the online version at [doi:10.1016/j.biopha.2022.114138](https://doi.org/10.1016/j.biopha.2022.114138).

References

- [1] D.B. Rein, J.S. Wittenborn, X. Zhang, A.A. Honeycutt, S.B. Lesesne, J. Saaddine, G. Vision, Health cost-effectiveness study, forecasting age-related macular degeneration through the year 2050: the potential impact of new treatments, *Arch. Ophthalmol.* 127 (4) (2009) 533–540.
- [2] J. Garcia-Garcia, R. Usategui-Martin, M.R. Sanabria, E. Fernandez-Perez, J. J. Telleria, R.M. Coco-Martin, Pathophysiology of age-related macular degeneration. implications for treatment, *Ophthalmic Res.* (2022).
- [3] A. Tisi, M. Feligioni, M. Passacantando, M. Ciancaglini, R. Maccarone, The impact of oxidative stress on blood-retinal barrier physiology in age-related macular degeneration, *Cells* 10 (1) (2021).
- [4] J. Ambati, B.J. Fowler, Mechanisms of age-related macular degeneration, *Neuron* 75 (1) (2012) 26–39.
- [5] S.A. Mousa, S.S. Mousa, Current status of vascular endothelial growth factor inhibition in age-related macular degeneration, *BioDrugs* 24 (3) (2010) 183–194.
- [6] M.M. Brown, G.C. Brown, J.D. Stein, Z. Roth, J. Campanella, G.R. Beauchamp, Age-related macular degeneration: economic burden and value-based medicine analysis, *Can. J. Ophthalmol.* 40 (3) (2005) 277–287.
- [7] A. Kauppinen, J.J. Paterno, J. Blasiak, A. Salminen, K. Kaarniranta, Inflammation and its role in age-related macular degeneration, *Cell Mol. Life Sci.* 73 (9) (2016) 1765–1786.
- [8] J. Kim, J.H. Kim, J.Y. Do, J.Y. Lee, R. Yanai, I.K. Lee, K. Suk, D.H. Park, Key role of microglial matrix metalloproteinases in choroidal neovascularization, *Front. Cell Neurosci.* 15 (2021), 638098.
- [9] L. Cao, H. Wang, F. Wang, D. Xu, F. Liu, C. Liu, Abeta-induced senescent retinal pigment epithelial cells create a proinflammatory microenvironment in AMD, *Invest Ophthalmol. Vis. Sci.* 54 (5) (2013) 3738–3750.
- [10] O. Tatar, A. Adam, K. Shinoda, T. Eckert, G.B. Scharioth, M. Klein, E. Yoeruek, K. U. Bartz-Schmidt, S. Grisanti, Matrix metalloproteinases in human choroidal neovascular membranes excised following verteporfin photodynamic therapy, *Br. J. Ophthalmol.* 91 (9) (2007) 1183–1189.
- [11] K.Y. Chau, S. Sivaprasad, N. Patel, T.A. Donaldson, P.J. Luthert, N.V. Chong, Plasma levels of matrix metalloproteinase-2 and -9 (MMP-2 and MMP-9) in age-related macular degeneration, *Eye* 22 (6) (2008) 855–859.
- [12] J.B. Jonas, Y. Tao, M. Neumaier, P. Findeisen, Cytokine concentration in aqueous humour of eyes with exudative age-related macular degeneration, *Acta Ophthalmol.* 90 (5) (2012) e381–e388.
- [13] S.M. Ecker, S.M. Pfahler, J.C. Hines, A.S. Lovelace, B.M. Glaser, Sequential in-office vitreous aspirates demonstrate vitreous matrix metalloproteinase 9 levels correlate with the amount of subretinal fluid in eyes with wet age-related macular degeneration, *Mol. Vis.* 18 (2012) 1658–1667.
- [14] N. Fiotti, M. Pedio, M. Battaglia Parodi, N. Altamura, L. Uxa, G. Guarnieri, C. Giansante, G. Ravalico, MMP-9 microsatellite polymorphism and susceptibility to exudative form of age-related macular degeneration, *Genet. Med.* 7 (4) (2005) 272–277.
- [15] V. Lambert, B. Wielockx, C. Munaut, C. Galopin, M. Jost, T. Itoh, Z. Werb, A. Baker, C. Libert, H.W. Krell, J.M. Foidart, A. Noel, J.M. Rakic, MMP-2 and MMP-9 synergize in promoting choroidal neovascularization, *FASEB J.* 17 (15) (2003) 2290–2292.
- [16] L. Guo, A.A. Hussain, G.A. Limb, J. Marshall, Age-dependent variation in metalloproteinase activity of isolated human Bruch's membrane and choroid, *Invest Ophthalmol. Vis. Sci.* 40 (11) (1999) 2676–2682.
- [17] S. Hoffmann, S. He, M. Ehren, S.J. Ryan, P. Wiedemann, D.R. Hinton, MMP-2 and MMP-9 secretion by rpe is stimulated by angiogenic molecules found in choroidal neovascular membranes, *Retina* 26 (4) (2006) 454–461.
- [18] A. Lommatzsch, P. Hermans, K.D. Muller, N. Bornfeld, A.C. Bird, D. Pauleikhoff, Are low inflammatory reactions involved in exudative age-related macular degeneration? Morphological and immunohistochemical analysis of AMD associated with basal deposits, *Graefes Arch. Clin. Exp. Ophthalmol.* 246 (6) (2008) 803–810.
- [19] M. Bandyopadhyay, B. Rohrer, Matrix metalloproteinase activity creates pro-angiogenic environment in primary human retinal pigment epithelial cells exposed to complement, *Invest Ophthalmol. Vis. Sci.* 53 (4) (2012) 1953–1961.
- [20] W. Ma, L. Zhao, A.M. Fontainhas, R.N. Fariss, W.T. Wong, Microglia in the mouse retina alter the structure and function of retinal pigmented epithelial cells: a potential cellular interaction relevant to AMD, *PLoS One* 4 (11) (2009), e7945.
- [21] W.C. Parks, C.L. Wilson, Y.S. Lopez-Boado, Matrix metalloproteinases as modulators of inflammation and innate immunity, *Nat. Rev. Immunol.* 4 (8) (2004) 617–629.
- [22] N. Gupta, K.E. Brown, A.H. Milam, Activated microglia in human retinitis pigmentosa, late-onset retinal degeneration, and age-related macular degeneration, *Exp. Eye Res.* 76 (4) (2003) 463–471.
- [23] E.B. Rodrigues, Inflammation in dry age-related macular degeneration, *Ophthalmologica* 221 (3) (2007) 143–152.
- [24] W. Ma, L. Zhao, W.T. Wong, Microglia in the outer retina and their relevance to pathogenesis of age-related macular degeneration, *Adv. Exp. Med Biol.* 723 (2012) 37–42.
- [25] J. Chen, L.C. Zhang, Y.M. Xing, Y.Q. Wang, X.K. Xing, D.W. Zhang, H.Q. Liang, S. X. Guo, Diversity and taxonomy of endophytic xylariaceae fungi from medicinal plants of Dendrobium (Orchidaceae), *PLoS One* 8 (3) (2013), e58268.
- [26] W.L. Liang, C.J. Hsiao, Y.M. Ju, L.H. Lee, T.H. Lee, Chemical constituents of the fermented broth of the ascomycete *Theissenia cinerea* 89091602, *Chem. Biodivers.* 8 (12) (2011) 2285–2290.
- [27] F.L. Lin, J.D. Ho, Y.W. Cheng, G.C.Y. Chiou, J.L. Yen, H.M. Chang, T.H. Lee, G. Hsiao, Theissenolactone C exhibited ocular protection of endotoxin-induced uveitis by attenuating ocular inflammatory responses and glial activation, *Front Pharm.* 9 (2018) 326.
- [28] F.L. Lin, Y.W. Cheng, M. Yu, J.D. Ho, Y.C. Kuo, G.C.Y. Chiou, H.M. Chang, T.H. Lee, G. Hsiao, The fungus-derived retinoprotectant theissenolactone C improves glaucoma-like injury mediated by MMP-9 inhibition, *Phytomedicine* 56 (2019) 207–214.
- [29] J.S. Jan, Y.C. Chou, Y.W. Cheng, C.K. Chen, W.J. Huang, G. Hsiao, The novel HDAC8 inhibitor WK2-16 attenuates lipopolysaccharide-activated matrix metalloproteinase-9 expression in human monocytic cells and improves hypercytokinemia in vivo, *Int. J. Mol. Sci.* 18 (7) (2017).
- [30] Y.C. Chou, J.R. Sheu, C.L. Chung, C.Y. Chen, F.L. Lin, M.J. Hsu, Y.H. Kuo, G. Hsiao, Nuclear-targeted inhibition of NF-kappaB on MMP-9 production by N-2-(4-bromophenyl) ethyl caffeine in human monocytic cells, *Chem. Biol. Inter.* 184 (3) (2010) 403–412.
- [31] R. Kannan, D.R. Hinton, Sodium iodate induced retinal degeneration: new insights from an old model, *Neural. Regen. Res.* 9 (23) (2014) 2044–2045.
- [32] J. Kinoshita, N.S. Peachey, Noninvasive electroretinographic procedures for the study of the mouse retina, *Curr. Protoc. Mouse Biol.* 8 (1) (2018) 1–16.
- [33] F.L. Lin, C.H. Lin, J.D. Ho, J.L. Yen, H.M. Chang, G.C. Chiou, Y.W. Cheng, G. Hsiao, The natural retinoprotectant chrysophanol attenuated photoreceptor cell apoptosis in an N-methyl-N-nitrosourea-induced mouse model of retinal degeneration, *Sci. Rep.* 7 (2017) 41086.
- [34] E. An, H. Gordish-Dressman, Y. Hathout, Effect of TNF-alpha on human ARPE-19-secreted proteins, *Mol. Vis.* 14 (2008) 2292–2303.
- [35] S. Mitchell, J. Vargas, A. Hoffmann, Signaling via the NFkappaB system, *Wiley Inter. Rev. Syst. Biol. Med* 8 (3) (2016) 227–241.
- [36] S.C. Cheng, Y.H. Wu, W.C. Huang, J.S. Pang, T.H. Huang, C.Y. Cheng, Anti-inflammatory property of quercetin through downregulation of ICAM-1 and MMP-9 in TNF-alpha-activated retinal pigment epithelial cells, *Cytokine* 116 (2019) 48–60.
- [37] M. Hollborn, C. Stathopoulos, A. Steffen, P. Wiedemann, L. Kohen, A. Bringmann, Positive feedback regulation between MMP-9 and VEGF in human RPE cells, *Invest. Ophthalmol. Vis. Sci.* 48 (9) (2007) 4360–4367.
- [38] P.L. Penfold, M.C. Madigan, M.C. Gillies, J.M. Provis, Immunological and aetiological aspects of macular degeneration, *Prog. Retin. Eye Res.* 20 (3) (2001) 385–414.
- [39] H. Kettenmann, U.K. Hanisch, M. Noda, A. Verkhratsky, Physiology of microglia, *Physiol. Rev.* 91 (2) (2011) 461–553.
- [40] H. Kohno, Y. Chen, B.M. Kevany, E. Pearlman, M. Miyagi, T. Maeda, K. Palczewski, A. Maeda, Photoreceptor proteins initiate microglial activation via Toll-like receptor 4 in retinal degeneration mediated by all-trans-retinal, *J. Biol. Chem.* 288 (21) (2013) 15326–15341.
- [41] H. Lassmann, J. van Horsen, Oxidative stress and its impact on neurons and glia in multiple sclerosis lesions, *Biochim Biophys. Acta* 1862 (3) (2016) 506–510.
- [42] M.H. Cheong, S.R. Lee, H.S. Yoo, J.W. Jeong, G.Y. Kim, W.J. Kim, I.C. Jung, Y. H. Choi, Anti-inflammatory effects of *Polygala tenuifolia* root through inhibition of NF-kappaB activation in lipopolysaccharide-induced BV2 microglial cells, *J. Ethnopharmacol.* 137 (3) (2011) 1402–1408.
- [43] A.W. Taylor, S. Hsu, T.F. Ng, The role of retinal pigment epithelial cells in regulation of macrophages/microglial cells in retinal immunobiology, *Front Immunol.* 12 (2021), 724601.
- [44] J.E. Grunwald, T.I. Metelitsina, J.C. Dupont, G.S. Ying, M.G. Maguire, Reduced foveolar choroidal blood flow in eyes with increasing AMD severity, *Invest Ophthalmol. Vis. Sci.* 46 (3) (2005) 1033–1038.

- [45] E. Buschini, A. Piras, R. Nuzzi, A. Vercelli, Age related macular degeneration and drusen: neuroinflammation in the retina, *Prog. Neurobiol.* 95 (1) (2011) 14–25.
- [46] R. Liutkeviciene, V. Liutkevicius, A. Giedraitiene, L. Kriauciuniene, V. Asmoniene, Influence of matrix metalloproteinases mmp-2, -3 and on age-related macular degeneration development, in: F. Traversio (Ed.), *The Role of Matrix Metalloproteinase in Human Body Pathologies*, IntechOpen, 2017.
- [47] L. Chen, N. Miyamura, Y. Ninomiya, J.T. Handa, Distribution of the collagen IV isoforms in human Bruch's membrane, *Br. J. Ophthalmol.* 87 (2) (2003) 212–215.
- [48] E. Hrabec, J. Naduk, M. Streck, Z. Hrabec, Type IV collagenases (MMP-2 and MMP-9) and their substrates—intracellular proteins, hormones, cytokines, chemokines and their receptors, *Post. Biochem.* 53 (1) (2007) 37–45.
- [49] A.J. Adler, C.D. Evans, Proteins of the bovine interphotoreceptor matrix: retinoid binding and other functions, *Prog. Clin. Biol. Res* 190 (1985) 65–88.
- [50] J. Kurzepa, J. Kurzepa, P. Golab, S. Czerska, J. Bielewicz, The significance of matrix metalloproteinase (MMP)-2 and MMP-9 in the ischemic stroke, *Int J. Neurosci.* 124 (10) (2014) 707–716.
- [51] P.E. Van den Steen, P. Proost, A. Wuyts, J. Van Damme, G. Opdenakker, Neutrophil gelatinase B potentiates interleukin-8 tenfold by aminoterminal processing, whereas it degrades CTAP-III, PF-4, and GRO-alpha and leaves RANTES and MCP-2 intact, *Blood* 96 (8) (2000) 2673–2681.
- [52] H. Zhao, J. Roychoudhury, T.A. Doggett, R.S. Apte, T.A. Ferguson, Age-dependent changes in FasL (CD95L) modulate macrophage function in a model of age-related macular degeneration, *Invest. Ophthalmol. Vis. Sci.* 54 (8) (2013) 5321–5331.
- [53] C.H. Wang, G.F. Cao, Q. Jiang, J. Yao, TNF-alpha promotes human retinal pigment epithelial (RPE) cell migration by inducing matrix metalloproteinase 9 (MMP-9) expression through activation of Akt/mTORC1 signaling, *Biochem. Biophys. Res. Commun.* 425 (1) (2012) 33–38.
- [54] M. Chen, H. Xu, Parainflammation, chronic inflammation, and age-related macular degeneration, *J. Leukoc. Biol.* 98 (5) (2015) 713–725.
- [55] H. Wang, X. Song, M. Li, X. Wang, Y. Tao, X. Xiya, H. Liu, Y. Zhao, D. Chang, Q. Sha, The role of TLR4/NF-kappaB signaling pathway in activated microglia of rats with chronic high intraocular pressure and vitro scratch injury-induced microglia, *Int. Immunopharmacol.* 83 (2020), 106395.
- [56] Y. Choi, M.K. Lee, S.Y. Lim, S.H. Sung, Y.C. Kim, Inhibition of inducible NO synthase, cyclooxygenase-2 and interleukin-1beta by torilin is mediated by mitogen-activated protein kinases in microglial BV2 cells, *Br. J. Pharm.* 156 (6) (2009) 933–940.
- [57] B.L. Wilkinson, G.E. Landreth, The microglial NADPH oxidase complex as a source of oxidative stress in Alzheimer's disease, *J. Neuroinflamm.* 3 (2006) 30.
- [58] S. Abokyi, C.H. To, T.T. Lam, D.Y. Tse, Central role of oxidative stress in age-related macular degeneration: evidence from a review of the molecular mechanisms and animal models, *Oxid. Med. Cell Longev.* 2020 (2020) 7901270.
- [59] D.M. Rabin, R.L. Rabin, T.A. Blenkinsop, S. Temple, J.H. Stern, Chronic oxidative stress upregulates Drusen-related protein expression in adult human RPE stem cell-derived RPE cells: a novel culture model for dry AMD, *Aging (Albany NY)* 5 (1) (2013) 51–66.
- [60] M.H. Madeira, K. Rashid, A.F. Ambrosio, A.R. Santiago, T. Langmann, Blockade of microglial adenosine A2A receptor impacts inflammatory mechanisms, reduces ARPE-19 cell dysfunction and prevents photoreceptor loss in vitro, *Sci. Rep.* 8 (1) (2018) 2272.
- [61] J. Hanus, C. Anderson, D. Sarraf, J. Ma, S. Wang, Retinal pigment epithelial cell necroptosis in response to sodium iodate, *Cell Death Disco* 2 (2016) 16054.
- [62] M.T. Pardue, N.S. Peachey, Mouse b-wave mutants, *Doc. Ophthalmol.* 128 (2) (2014) 77–89.
- [63] Z. Burgansky-Eliash, H. Barash, D. Nelson, A. Grinvald, A. Sorkin, A. Loewenstein, A. Barak, Retinal blood flow velocity in patients with age-related macular degeneration, *Curr. Eye Res.* 39 (3) (2014) 304–311.
- [64] E. Friedman, S. Krupsky, A.M. Lane, S.S. Oak, E.S. Friedman, K. Egan, E. S. Gragoudas, Ocular blood flow velocity in age-related macular degeneration, *Ophthalmology* 102 (4) (1995) 640–646.